2015

Femtosecond laser induced tunable surface transformations on (111) Si aided by square grids diffraction

Weina Han
Laser Micro/Nano-Fabrication Laboratory, School of Mechanical Engineering, Beijing Institute of Technology, Beijing

Lan Jiang
Laser Micro/Nano-Fabrication Laboratory, School of Mechanical Engineering, Beijing Institute of Technology, Beijing

Xiaowei Li
Laser Micro/Nano-Fabrication Laboratory, School of Mechanical Engineering, Beijing Institute of Technology, Beijing, lixiaowei@bit.edu.cn

Yang Liu
Laser Micro/Nano-Fabrication Laboratory, School of Mechanical Engineering, Beijing Institute of Technology, Beijing

Yongfeng Lu
University of Nebraska-Lincoln, ylu2@unl.edu

Femtosecond laser induced tunable surface transformations on (111) Si aided by square grids diffraction

Weina Han,[1] Lan Jiang,[1] Xiaowei Li,[1,a)] Yang Liu,[1] and Yongfeng Lu[2]
[1]*Laser Micro/Nano-Fabrication Laboratory, School of Mechanical Engineering, Beijing Institute of Technology, Beijing 100081, People's Republic of China*
[2]*Department of Electrical Engineering, University of Nebraska-Lincoln, Lincoln, Nebraska 68588-0511, USA*

(Received 16 September 2015; accepted 8 December 2015; published online 21 December 2015)

We report an extra freedom to modulate the femtosecond laser energy distribution to control the surface ablated structures through a copper-grid mask. Due to the reduced deposited pulse energy by changing the scanning speed or the pulse fluence, a sequential evolution of three distinctly different surface patterns with periodic distributions is formed, namely, striped ripple lines, ripple microdots, and surface modification. By changing the scanning speed, the number of the multiple dots in a lattice can be modulated. Moreover, by exploring the ablation process through the copper grid mask, it shows an abnormal enhanced ablation effect with strong dependence of the diffraction-aided fs laser ablated surface structures on polarization direction. The sensitivity shows a quasi-cosinusoid-function with a periodicity of $\pi/2$. Particularly, the connection process of striped ripple lines manifests a preferential formation direction with the laser polarization. © *2015 AIP Publishing LLC*.
[http://dx.doi.org/10.1063/1.4938244]

Surface micro/nano-structures on bulk solids with controllable morphologies and arrangements have been attracting great attention due to their scientific and technological properties in controlling optical,[1,2] mechanical,[3] wetting,[1,4] chemical,[5] biological,[6] and other properties. Significant effort has been devoted to the exploration of effective approaches for realizing various controllable surface patterning. Laser treatment is one of the main techniques for designing nano- and microstructures due to its excellent controllability of the surface micro/nanostructures compared to other processes.[2,7–9] Especially in recent years, femtosecond (fs) laser surface micro/nanostructuring has been demonstrated as a versatile technology for producing a large variety of micro/nanostructured materials suitable for a wide range of applications.[10–12]

It has been shown that it is possible to pattern nanostructured films by irradiating thin films on solid substrates by a diffraction controlled nonuniform laser beam irradiation.[13,14] More recently, investigations reveal that extra-assisted means can be used to manipulate the surface micro/nanostructures under fs laser irradiation. For example, Shen *et al.* reported the fabrication of regular arrays of silicon microspikes by fs laser irradiation through a mask.[15] Zywietz *et al.* demonstrated a laser printing technique for fabricating periodic arrays of silicon nanoparticles.[16] Wang *et al.* reported a micro/nanopatterning by fs laser irradiation through a pinhole.[17] Two of the essential challenges of laser induced surface micro/nanostructures are the control of the morphologies of the individual objects and the control of their arrangements.

Here, we report the observation of fs laser induced surface transformation modulation through a copper mask. The experimental results demonstrate a sequential evolution of striped ripple lines, ripple microdots, and surface modification formation by deliberately modulating the scanning speed or the pulse fluence at the fixed diffraction distance. Meanwhile, the minimum number of the multiple dots by varying the scanning speed shows close correspondence with the simulation result based on a semi-quantitative Fresnel diffraction model. An abnormal enhancement ablation characteristic with a polarization-dependent sensitivity is observed, and it exhibits a quasi-cosinusoid-function distribution with a $\pi/2$ periodicity.

The experimental setup (Fig. 1) is similar to that in our previous studies.[18] The fs laser pulse (1 kHz, $\tau = 50$ fs (FWHM), and $\lambda = 800$ nm) travels through the dichroic mirror (DM) and is focused through an achromatic doublet ($f = 100$ mm) on the surface of standard one-side-polished p-type (111) Si chip (10 mm × 10 mm × 1 mm). The focus point is set on the surface by moving the sample along the z-direction until the damage on the surface is most severe. The focal spot size (width at the waist defined by $1/e^2$ point) of the Gaussian beam is measured as 30 μm. As shown in Fig. 1

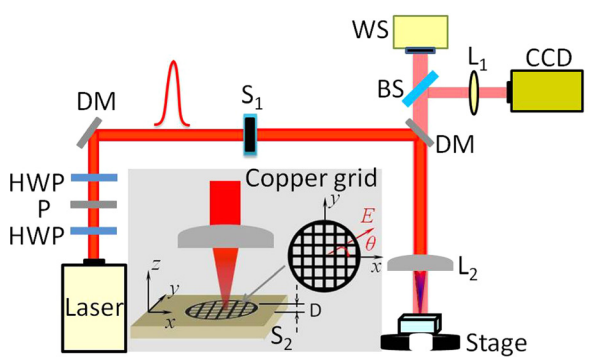

FIG. 1. Schematic diagram of the optical setup. Inset depicts the relative angle (θ) between directions of the linearly polarized fs laser and the sample coordinate. The red arrow represents the linear polarization direction of fs laser. HWP: half-wave plate; P: polarizer; S_1: shutter; WS: white-light source; BS: beam splitter; L_1: convex lens; DM: dichroic mirror; L_2: achromatic doublet; S_2: sample.

a)Electronic mail: lixiaowei@bit.edu.cn.

inset, a square copper grid with one edge of the gird parallel to the x-axis is affixed on the surface of the sample with conductive carbon tape. The scanning direction is fixed along the x-axis. θ is defined as the relative angle between the laser polarization direction and the x-axis and D is the diffraction distance between copper mask and the sample surface. The square opening grid is 30-μm-thick and 19-μm-width, and the center distance between two adjacent grids is 25 μm. All experiments are performed in air at room temperature under normal incidence. After irradiation, the mask is removed and the resulting surface morphology is characterized by a scanning electron microscope (SEM).

For suitable pulse energies and scanning speeds, the sample surface will appear with three typical morphologies. Figs. 2(a)–2(f) are the diffraction-aided fs laser ablated structures with different scanning speeds (v) of 100 μm/s, 300 μm/s, 400 μm/s, 500 μm/s, 600 μm/s, and 700 μm/s, respectively. The laser fluence is 0.15 J/cm^2. By reducing deposited laser energy, an evolution of striped ripple lines, ripple microdots, and surface modification is formed as the scanning speed increases. As shown, a 4×4 lattice of ripples (the black dotted line marked-area, Figs. 2(b) and 2(g)) with the spacing of the two adjacent dots of $\sim 2.5 \pm 0.5$ μm can be observed with $v = 200$ μm/s. For $v = 300$ μm/s, the magnitude of the dots decreases (Fig. 2(c)) while the spacing keeps nearly unchanged. A 5×5 lattice of ripples is formed when $v = 500$ μm/s with the adjacent spacing decreasing to $\sim 2 \pm 0.5$ μm, as shown in Fig. 2(d). The number of the dots in a lattice keeps increasing to 6×6 with the adjacent spacing decreasing to $\sim 1.5 \pm 0.5$ μm when $v = 600$ μm/s. Increase v to 700 μm/s, a new transformation of surface modification appears with a 7×7 lattice distribution. And the adjacent spacing is decreased to $\sim 1 \pm 0.5$ μm. After the laser pulse propagates through the diffraction aperture, the energy distribution of laser pulse presents periodicity variation in spatial. Surface modification is formed when the peak fluence of the periodically deposited laser energy is below the ablation threshold. With increase of the deposited pulse energy, surface plasmon polaritons (SPPs) are excited when the periodically redistributed areas turn to a metallic state[19–21] and subsequent interference between its electrical field with that of the incident laser beam resulting in the periodic ripple structure formation.[22,23] Furthermore, it can be seen that multiple dots near the grid lines are larger than that in the central area. This indicates that the energy density at the grid lines is greater. Especially, the striped ripple lines are supposed to be a connection between the ripple microdots when the scanning speed is relatively low (Fig. 2(a)), and the detailed impact factor will be described further later.

A semi-quantitative Fresnel diffraction model (see supplementary material[24] Section F) is used to analyze the diffraction characteristics induced by a square aperture.[25] By solving the Fresnel diffraction equations (Equation (S6) in the supplementary material[24]), we can get the intensity distribution. For $D = 25$ μm, the corresponding calculated relative intensity distribution is presented in Fig. 2(h) as a function of the horizontal position in the surface plane. One can observe the minimum number of the multiple dots by varying the scanning speed, which shows a close correspondence with the simulation result. Some typical results with different D are shown in Figs. 3(a), 3(c), 3(e), and 3(f). 3×3, 4×4, 5×5, and 6×6 lattice intensity distribution can be clearly identified with $D = 20$ μm, $D = 25$ μm, $D = 30$ μm, and $D = 35$ μm, respectively. It implies that the number of the micro-peak intensities increases as D increases. To confirm the effect of diffraction distance on the distribution of the optical field, a reduced distance of $D \approx 20$ μm by placing the

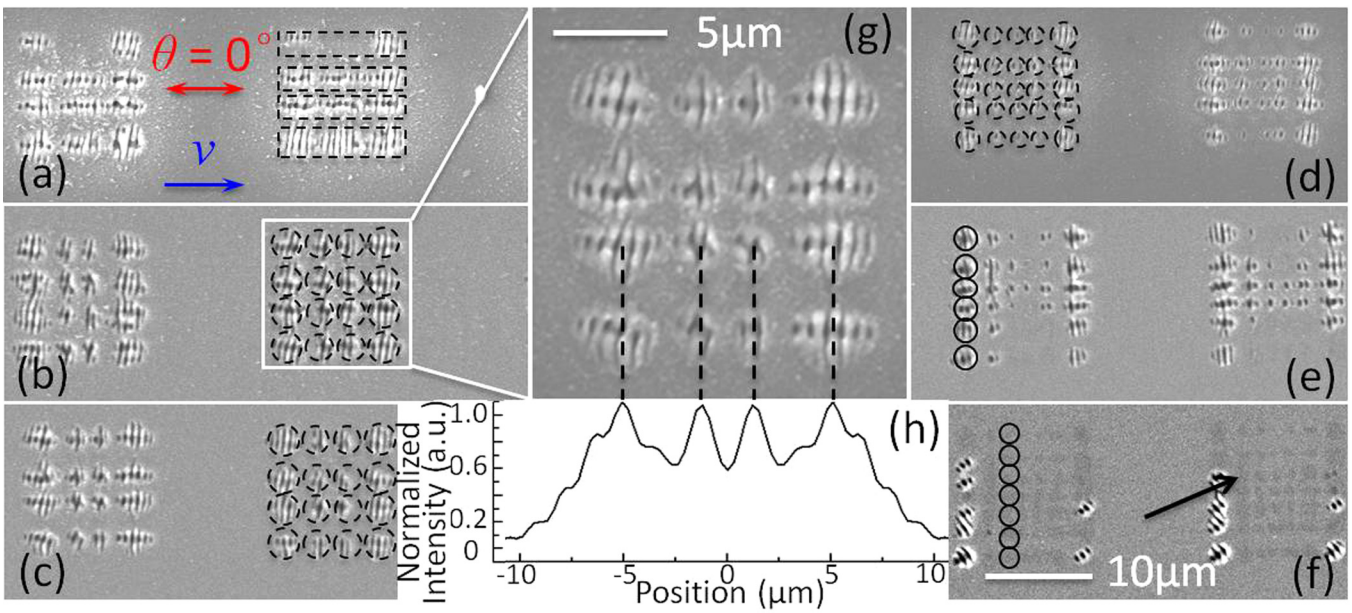

FIG. 2. (a)–(f) SEM images of the fs laser irradiated spots through the square copper grids in different scanning speeds. (a) 100 μm/s; (b) 300 μm/s; (c) 400 μm/s; (d) 500 μm/s; (e) 600 μm/s; (f) 700μm/s. Inset (g) shows a magnification of 4×4 lattice dots in (b); (h) the corresponding calculated normalized electric field distribution with a 4×4 lattice. An arrow in (f) is provided to assist the reader in locating the surface modification; the red double-headed arrow and blue arrow indicate the polarization direction and the scanning direction, respectively. The polarization direction and the scanning direction are fixed from (a) to (f).

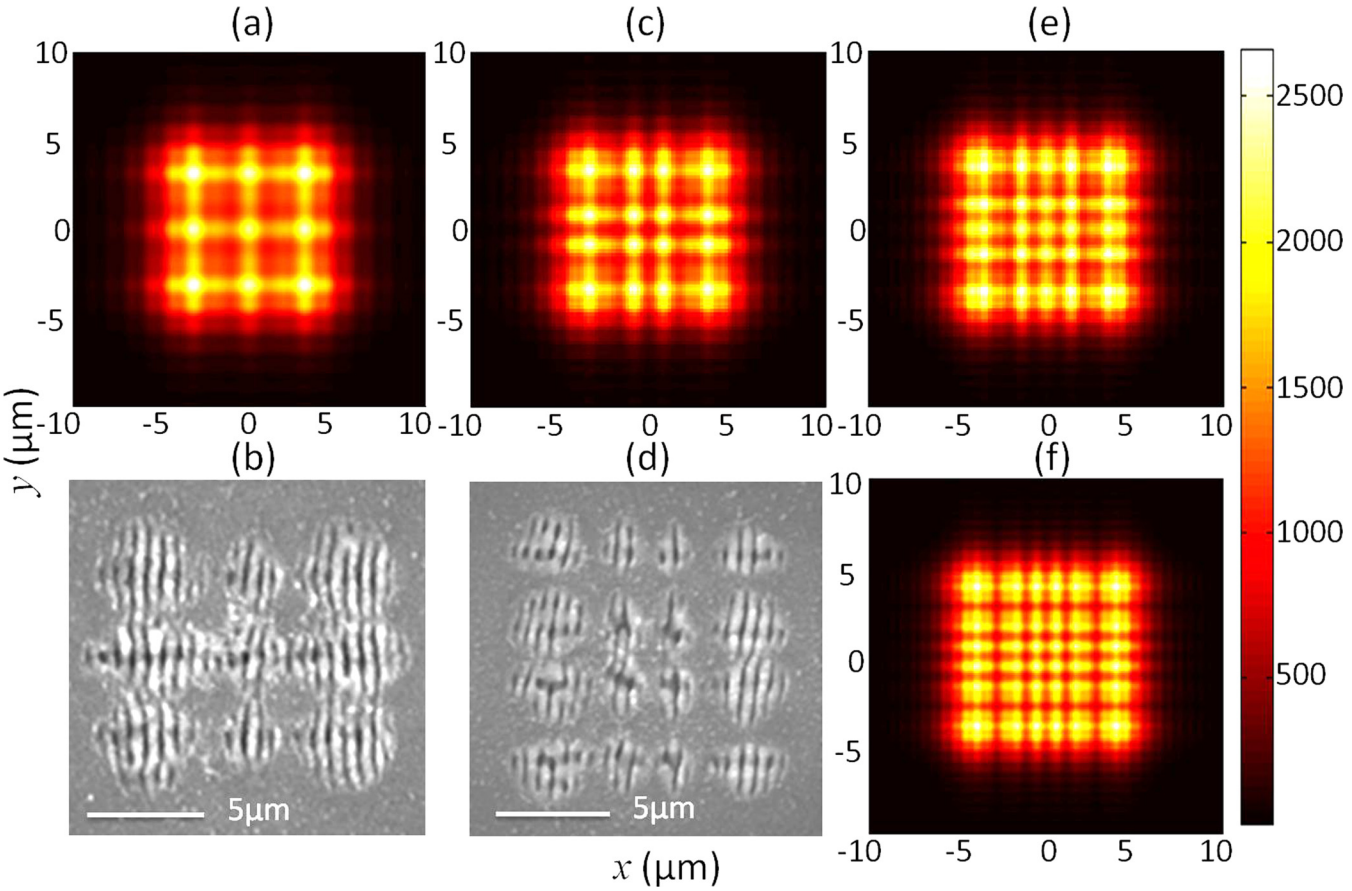

FIG. 3. The numerical calculated electric field distributions through the square aperture on the surface of the sample with different D: (a) 20 μm; (c) 25 μm; (e) 30 μm; (f) 35 μm. (b) and (d) SEM images of 3×3 lattice with D around 20 μm and 4×4 lattice with D around 25 μm, respectively. The scanning speed is 200 μm/s and 300 μm/s, respectively.

copper grids tightly on the surface of sample (Fig. S1 in the supplementary material[24]) is performed. The minimum number of the multiple dots of 3×3 lattice ($D \approx 20\,\mu$m) and 4×4 lattice ($D \approx 25\,\mu$m) is shown in Figs. 2(b) and 2(d), respectively. The separation width in the horizontal and vertical directions of the minimum number of the multiple dots array with fixed D shows a good correspondence with the semi-quantitative theoretical simulations.

The aforementioned results demonstrate an abnormal phenomenon that the number of the multiple dots can be controlled by changing the laser scanning parameters under fixed diffraction distance. This is not consistent with the previous classical theory of Fresnel diffraction that the diffraction pattern is determined by the diffraction distance.[25] The formation of the multiple dots can be considered as the repetition of the two-step process (as shown in Fig. S2 in the supplementary material[24]). We deduce that the control of the number of the multiple dots in a lattice by the scanning speed is mainly attributed to the overlap during the scanning process. When the fs laser is irradiated on the sample surface through the copper grid, initially seeding diffracted multiple ripple dots is induced. The overlap areas and positions between the seeding ripple dots and irradiation beam change with the scanning speed, which could affect the subsequent multiple dots distribution under certain conditions (Fig. S2(b)–S2(f)). This effect plays a dominant role for the subsequent multiple dots formation. Moreover, it may be also related to the SPP. Previous researches reveal that initially structured surface could affect the generation and propagation of the SPP.[20,21,26] Hence, when the laser beam irradiates on certain positions of the initial diffracted structure, the coupling between the specially excited SPP and the irradiation laser beam may result in the subsequent multiple dots arrays. However, the exact mechanism for this phenomenon is still unclear and needs more investigations.

In the following, we compare the fs laser ablation through the copper mask to that without copper mask. Fig. 4(a) gives SEM image of the surface ablation induced by fs laser scanning with/without (left/right) mask at different pulse energies. Certain pulse energy irradiated area under these two conditions is marked with dotted lines with the same color. For $F = 0.1\,\text{J/cm}^2$ (marked by red-dotted lines), no transformation takes place without the mask. Increasing F, surface transformation only occurs for large pulse energy ($F = 0.2\,\text{J/cm}^2$, marked by blue-dotted lines; $F = 0.3\,\text{J/cm}^2$, marked by black-dotted lines) higher than the ablation threshold at certain scanning speed without the mask, whereas obvious transformation takes place with the mask, as can be illustrated by the strong visual contrast. This illustrates an ablation enhancement effect induced by the diffraction-aided fs laser irradiation. The Gaussian distribution of the optical field turns into a more concentrated periodical optical field distribution (Fig. 3) through the square grids. It is supposed that the concentrated redistributed

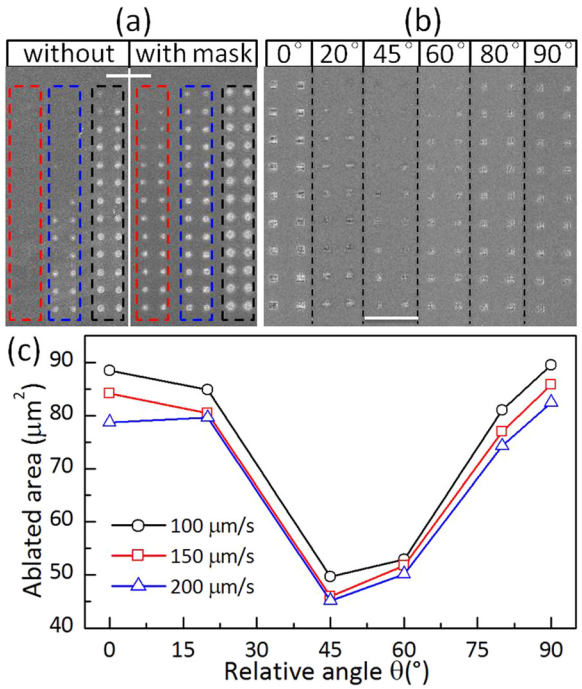

FIG. 4. (a) SEM image of the fs laser irradiated spots without (left)/with (right) assisted mask at different pulse energies: the scale bar is 100 μm. (b) SEM image of mask-assisted diffracted structures with different relative angles. From bottom to top, the scanning speed is increased from $v = 100\,\mu$m/s to $v = 500\,\mu$m/s and the scale bar is 100 μm. (c) The corresponding ablated area is shown as a function of relative angle from 0° to 90°.

optical field leads to the concentrated SPP excitation[21–23] and coupling with the incident light plays a key role in the enhanced ablation effect.

We also examine the influence of the laser polarization direction on the surface transformation through diffraction-aided fs laser irradiation. In Fig. 4(b), the incident pulse fluence presented is 0.15 J/cm^2. θ is changed from 0° to 90° with v increasing from 100 μm/s to 500 μm/s. Similarly, ripples are observed (the detailed structures are not shown here). At different scanning speeds, the grid-aided fs laser irradiated spots show nearly identical visual contrast when the relative angle changes from 0° to 90°. With fixed scanning speed, for example, of $v = 500\,\mu$m/s, obvious ablation occurs when the polarization direction is aligned with specific directions ($\theta = 0°$, 80°, and 90°), whereas no obvious modification is observed for θ of 20°, 45°, and 60°. The corresponding ablated area is measured as a function of the relative angle to quantitatively represent this certain polarization-sensitivity level. As shown in Fig. 4(c), the ablated area monotonously increases as the scanning speed decreases at identical relative angle, which is due to the increase of the deposited laser energy per unit area.[27] At the fixed scanning speed, the ablated area exhibits a quasi-cosinusoid dependent behavior on θ with a $\pi/2$ modulation periodicity. When the polarization direction is aligned with the orthogonal edge, it results in the maximum ablated area, while the polarization direction parallel to the diagonal line of the grid ($\theta = 45°$) results in the minimum ablated area. Intensity measurements reveal that no significant changes are observed. Meanwhile, no anisotropic ablation phenomenon under linearly polarized fs laser irradiation is found on the surface of (111) Si.[18,28] An anisotropic formation of ripples based on the crystal orientations has been found on the surface of (100) Si with cubic crystal structure due to the direction dependence of the effective mass of electron.[28] Here, the aided square grid can be seen as an additional quasi-cubic crystal structure added to the (111) Si surface. The transverse magnetic (TM) launching and directional scattering of SPPs are proposed to be responsible for this polarization-dependent ablation effect. Directional SPP scattering along the polarization direction by the initially formed ripple structures can be achieved under linearly polarized fs laser irradiation.[18] Meanwhile, the intrinsic TM state of the SPP field leads to a TM incidence for the SPP launching.

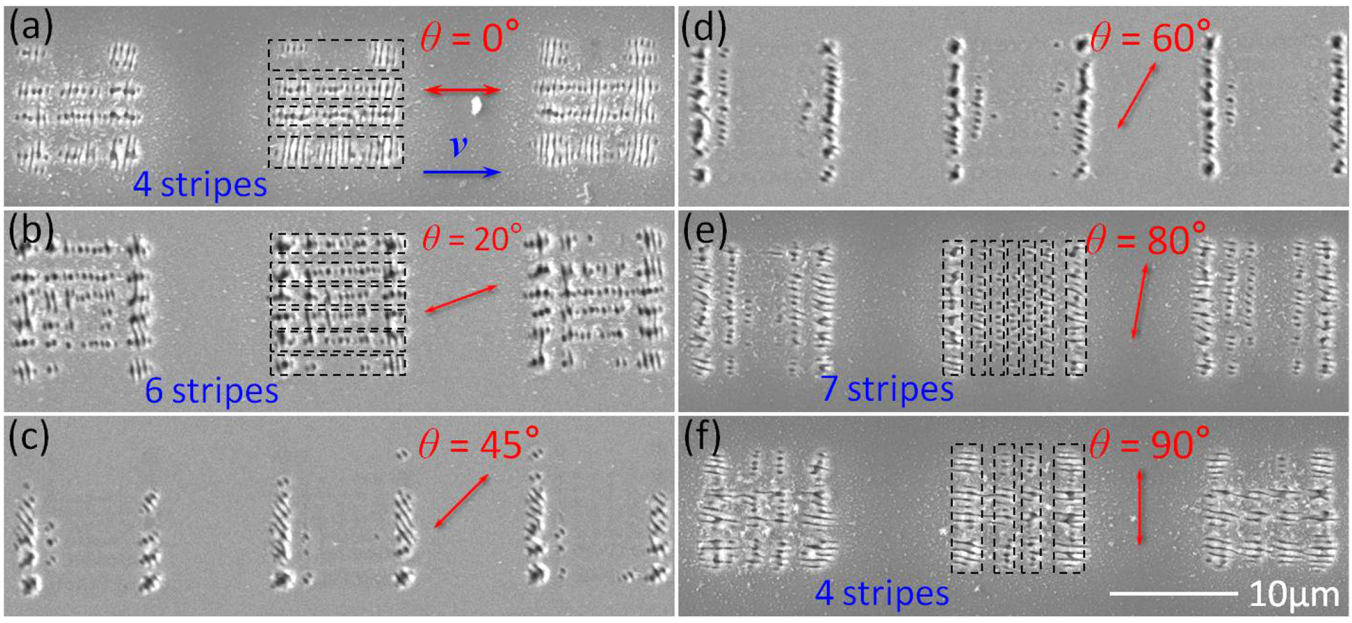

FIG. 5. (a)–(f) SEM images of mask-assisted diffracted structures with different relative angles at $v = 100\,\mu$m/s. The red double-headed arrow and blue arrow indicate the polarization direction and the scanning direction, respectively. The scanning direction is fixed. All the images share the same scale bar.

Thus, the SPP launching and coupling is perpendicular to the ripple structures (see Fig. S3 in the supplementary material[24] for the schematic illustration). The ablation of the multiple dots reaches the maximum by the overlap of the directional SPP launching and coupling when the polarization direction is along the orthogonal edge of the square aperture ($\theta = 0°/90°$), while with a minimum when the polarization direction is aligned with the diagonal line of the aperture ($\theta = 45°$).

Besides the polarization-dependent sensitivity effect, the polarization direction is also demonstrated to be a key parameter for the striped ripple lines formation. Fig. S4 in supplementary material[24] shows the striped ripple lines formation process. The direction of striped ripple lines is along one edge of the square grid. This is because the periodic striped ripple lines can be regarded as a connection of the separate ripple dots. Meanwhile, a change of the direction occurs when the polarization direction turns 90° around. This demonstrates the polarization direction maybe a key factor for the orthogonal directions selection. Figs. 5(a)–5(f) describe the transformation of the striped ripple lines under different laser polarization directions with $v = 100\ \mu$m/s. As expected, the formation of the periodic structures exhibits a polarization-dependent effect. It can be easily found that the striped ripple lines can be only found at certain angles of 0°, 20°, 80°, and 90°, whereas no regular structures (Figs. 5(c) and 5(d)) are found when the polarization direction is around the diagonal line of the square aperture. For relatively small angles ($\theta < 45°$), the direction of the stripes is along the horizontal direction, while turns around when $\theta > 45°$. Fig. S5 in supplementary material[24] illustrates the corresponding schematic diagram for the striped ripple lines direction selection. An elliptical shape of the ripple structure along the polarization direction can be achieved under linearly polarized fs laser irradiation.[18] Reduce the scanning speed, the increased laser energy leads to the reduction of the distance between the two adjacent ripple dots. Thus, the orthogonal periodic ripple dots with the minimum adjacent spacing are apt to be connected to stripe ripple lines when the polarization direction is near the horizontal or vertical directions.

In summary, we have demonstrated a tunable surface transformation by modulating the fs laser energy distribution through a diffracting copper grid mask. Three different surface transformations with controllable arrangement can be achieved by suitable scanning speeds and pulse fluence. The number of the multiple dots increases as the scanning speed increases. We attributed this abnormal phenomenon to the structures induced on the initial stage in the scanning process, which may act as seeds for subsequent multiple dots fabrication. An ablation enhancement effect is observed through the copper mask, and the ablation shows a quasi-cosinusoid-function to the relative angle (θ) between the polarization direction and the edge of the square aperture with a $\pi/2$ periodicity. Moreover, the surface striped ripple lines connected by the desperate multiple dots are also found to be sensitive to the laser polarization directions. The enhanced energy absorption along the laser polarization direction and the elliptical morphology induced by the enhanced SPP scattering along the polarization direction are proposed to be responsible for the selective connected directions of the striped ripple lines. This research demonstrates an extra feasibility and tunability of surface micro/nanostructures patternings under the irradiation of fs laser pulse, which show great potentials for precision machining and micro/nano-fabrication.

This research was supported by the National Basic Research Program of China (973 Program) (Grant No. 2011CB013000), National Natural Science Foundation of China (NSFC) (Grant Nos. 91323301 and 51305030), and the Specialized Research Fund for the Doctoral Program of Higher Education (Grant No. 20131101120018).

[1]K. C. Park, H. J. Choi, C. H. Chang, R. E. Cohen, G. H. McKinley, and G. Barbastathis, ACS Nano **6**, 3789–3799 (2012).
[2]C. Y. Zhang, J. W. Yao, H. Y. Liu, Q. F. Dai, L. J. Wu, S. Lan, V. A. Trofimov, and T. M. Lysak, Opt. Lett. **37**, 1106–1108 (2012).
[3]I. Etsion, Tribol. Lett. **17**, 733–737 (2004).
[4]S. Moradi, S. Kamal, P. Englezos, and S. G. Hatzikiriakos, Nanotechnology **24**, 415302 (2013).
[5]C. H. Crouch, J. E. Carey, J. M. Warrender, M. J. Aziz, E. Mazur, and F. Y. Génin, Appl. Phys. Lett. **84**, 1850 (2004).
[6]W. He, K. E. Gonsalves, N. Batina, D. B. Poker, E. Alexander, and M. Hudson, Biomed. Microdevices **5**, 101–108 (2003).
[7]A. Vorobyev and C. Guo, Appl. Phys. Lett. **92**, 041914 (2008).
[8]T. W. Ebbesen, H. J. Lezec, H. F. Ghaemi, T. Thio, and P. Wolff, Nature **391**, 667–669 (1998).
[9]T. Baldacchini, J. E. Carey, M. Zhou, and E. Mazur, Langmuir **22**, 4917–4919 (2006).
[10]Q. Wang, J. Maddock, E. T. F. Rogers, T. Roy, C. Craig, K. F. Macdonald, D. W. Hewak, and N. I. Zheludev, Appl. Phys. Lett. **104**, 121105 (2014).
[11]H. Yuan, V. Yost, M. Page, P. Stradins, D. Meier, and H. Branz, Appl. Phys. Lett. **95**, 123501 (2009).
[12]J. W. Chan, T. R. Huser, S. H. Risbud, J. S. Hayden, and D. M. Krol, Appl. Phys. Lett. **82**, 2371 (2003).
[13]E. Haro-Poniatowski, E. Fort, J. P. Lacharme, and C. Ricolleau, Appl. Phys. Lett. **87**, 143103 (2005).
[14]O. V. Overschelde and M. Wautelet, Appl. Phys. Lett. **89**, 161114 (2006).
[15]M. Y. Shen, C. H. Crouch, J. E. Carey, R. Younkin, E. Mazur, M. Sheehy, and C. M. Friend, Appl. Phys. Lett. **82**, 1715 (2003).
[16]U. Zywietz, A. B. Evlyukhin, C. Reinhardt, and B. N. Chichkov, Nat. Commun. **5**, 3402 (2014).
[17]S. T. Wang, G. Y. Feng, and S. H. Zhou, Appl. Phys. Lett. **105**, 253110 (2014).
[18]W. N. Han, L. Jiang, X. W. Li, P. J. Liu, L. Xu, and Y. F. Lu, Opt. Express **21**, 15505–15513 (2013).
[19]J. Bonse, A. Rosenfeld, and J. Krüger, J. Appl. Phys. **106**, 104910 (2009).
[20]S. A. Maier, *Plasmonics: Fundamentals and Applications* (Springer, 2007).
[21]W. L. Barnes, A. Dereux, and T. W. Ebbesen, Nature **424**, 824 (2003).
[22]T. J. Y. Derrien, J. Krüger, T. E. Itina, S. Höhm, A. Rosenfeld, and J. Bonse, Opt. Express **21**, 29643–29655 (2013).
[23]M. Huang, F. Zhao, Y. Cheng, N. Xu, and Z. Xu, ACS Nano **3**, 4062 (2009).
[24]See supplementary material at http://dx.doi.org/10.1063/1.4938244 for details of additional experimental results, schematic diagrams, striped ripple lines connection, and Fresnel diffraction by square aperture.
[25]F. He, H. Xu, Y. Cheng, J. L. Ni, H. Xiong, Z. Z. Xu, K. Sugioka, and K. Midorikawa, Opt. Lett. **35**, 1106–1108 (2010).
[26]P. J. Liu, L. Jiang, J. Hu, S. Zhang, and Y. F. Lu, Opt. Express **22**, 16669–16675 (2014).
[27]J. Bonse and J. Krüger, J. Appl. Phys. **108**, 034903 (2010).
[28]L. Jiang, W. N. Han, X. W. Li, Q. S. Wang, F. T. Meng, and Y. F. Lu, Opt. Lett. **39**, 3114–3117 (2014).